Use IAST with MPSD to Predict Binary Adsorption Kinetics on Activated Carbon

Shizhang Qiao and Xijun Hu
Dept. of Chemical Engineering, Hong Kong University of Science and Technology, Clear Water Bay, Kowloon, Hong Kong

A model using the ideal adsorbed solution theory (IAST) coupled with the micropore-size distribution (MPSD) concept is proposed to describe the multicomponent adsorption equilibrium and kinetics of gases in activated carbon. To overcome the thermodynamic violation, the IAST instead of the extended Langmuir equation was used to calculate the local multicomponent adsorption equilibrium. The micropore size is related to the adsorbate–adsorbent interaction energy by the Lennard-Jones potential. The overall adsorption isotherm and the diffusion flux of the adsorbed species are the integrals of their corresponding local values over all micropore-size distribution range accessible by the adsorbate molecules. The size exclusion effect was taken into account in the competition of different sized molecules for a given pore. The model predictions were tested with the adsorption kinetics data of binary gases on Ajax and Norit activated carbon. The results were better than predictions of a previous multicomponent adsorption kinetics model also using the MPSD concept, but with the local multicomponent adsorption isotherm described by the extended Langmuir equation.

Introduction

Modeling of multicomponent adsorption equilibrium and kinetics is crucial to the design and scale-up of practical adsorption processes. Among various theories of being able to predict mixed-gas adsorption equilibrium, the ideal adsorbed solution theory (IAST) has the advantages that no mixture data are required and no restriction exists for the type of pure-component isotherm equation (Myers and Prausnitz, 1965; Malek and Farooq, 1996). However, the original IAST failed to consider the nonideal behavior of the adsorbed phase. Sircar (1995) demonstrated that a large difference in molecular size and adsorbent heterogeneity can cause the erroneous predictions of IAST. Dunne and Mayer (1994) studied molecules of unequal size adsorbing into a microporous cavity by the computer simulation technique, and they found that the micropore-size exclusion effect for larger molecules generates nonideal behaviors of the system. A number of studies assumed some kind of energy distribution function, such as the uniform or binomial distribution, to address the adsorbent heterogeneity. With this assumption, the matching energies between different species can be decided by the cumulative energy matching scheme (Valenzuela et al., 1988; Moon and Tien, 1988; Kapoor et al., 1990; Hu and Do, 1995a). However, these distribution functions are oversimplified for real systems and the cumulative energy-matching scheme also suffers from the drawback that it cannot bring out the physical realities of competition between different adsorbates in the microporous network of adsorbent. That is, matching the energy of two species this way may occur over two pores of different size, which is physically impossible. Another disadvantage associated with the energy distribution concept is that the size exclusion effect cannot be considered. In order to overcome these drawbacks, some researchers utilized the pore-size distribution concept to describe the surface heterogeneity in the prediction of multicomponent adsorption equilibrium (Hu and Do, 1996; Wang and Do, 1997; Hu, 1999; Qiao et al., 2000a) and kinetics (Do and Wang, 1998a,b; Hu et al., 1999; Qiao and Hu, 2000). By assuming that the micropore-size distribution is the intrinsic property of adsorbent and the sole source of system heterogeneity, the adsorbate–adsorbent interaction can then be described by the Lennard-Jones potential theory (Everett and Powl, 1976; Jagiello and Schwarz, 1992, 1993). This method has two dis-

Correspondence concerning this article should be addressed to X. Hu.

tinguishing features. The competition between different adsorbates is confined within the same pore where they are accommodated, that is, adsorbates inaccessible to a pore do not participate in the competition and hence are not accounted for in the calculation of local equilibrium and the diffusion flux of adsorbed species for that pore. So the size exclusion effect is taken into account by this method. The other advantage is that the matching energies between different species are related to their own interaction strength with the local micropores. In micropores of different sizes, the local interaction energy is a function of not only the size of the micropore but also of the size of the adsorbate molecule. So this method sets a physical criterion for the local matching energies between different adsorbate molecules in the micropore. However, for the research done so far with the micropore-size distribution (MPSD) approach, an extended Langmuir equation (EL) was used to describe the local multicomponent adsorption equilibrium. This is referred to as MPSD-EL model. When the difference between the saturation capacities of various species is large, the extended Langmuir equation does not satisfy the thermodynamic consistency and causes serious deviation in the prediction of adsorption equilibrium and kinetics (Hu and Do, 1995a; Qiao and Hu, 2000; Qiao et al., 2000a). In order to overcome the thermodynamic violation and maintain a good fitting for single-component adsorption isotherm, we recently proposed a new multicomponent adsorption equilibrium model by assuming a micropore-size distribution to represent the energetic heterogeneity of the adsorbent and using the ideal adsorbed solution theory to describe the local multicomponent adsorption equilibrium within a given pore (Qiao et al., 2000b; Wang et al., 2000). This is called the MPSD-IAST model, which is thermodynamically consistent and has no limitations on the single-component isotherm fitting. In this study, we further extend this method to predict multicomponent adsorption kinetics. The model is examined against binary adsorption kinetics data of ethane and propane on two commercial activated carbons (Ajax and Norit). The prediction results also are compared with those obtained using the MPSD-EL model (Hu et al., 1999).

Theory

Let us consider a gas-mixture stream containing NC components. At time $t = 0$, a large microporous particle is exposed to this environment and the diffusion and adsorption processes are started. The flow rate of the gas stream is so high that the gas concentration can be considered constant and the system can be assumed isothermal (Hu and Do, 1995b). The adsorbent particle is assumed large enough so that the mass-transfer resistance is along the particle coordinator. Both pore and surface diffusions occur inside the particle. The adsorbed species are in local equilibrium with those in the gas phase, and the equilibrium can be expressed by the IAST.

Adsorption isotherm and adsorption energy

In this study, the gas–solid potential of a molecule confined in two parallel lattice planes is expressed by the well-known Lennard-Jones 10-4 potential (Everett and Powl, 1976):

$$u_p(k,z) = u_s^*(k)\frac{5}{3}\left\{\frac{2}{5}\left(\frac{r_0(k)}{z}\right)^{10} - \left(\frac{r_0(k)}{z}\right)^4 + \frac{2}{5}\left(\frac{r_0(k)}{2r_p - z}\right)^{10} - \left(\frac{r_0(k)}{2r_p - z}\right)^4\right\}, \quad (1)$$

where the parameter u_s^* is the depth of the Lennard-Jones potential minimum for a single lattice plane; r_p is the length between the pore center and a given atom of pore surface layer, or, the pore half-width plus the lattice half-space between graphite planes; z is the center–center distance between an adsorbate molecule and one side of the graphite lattice plane (pore wall); and r_0 is the collision diameter between an adsorbate molecule and a carbon molecule (Everett and Powl, 1976):

$$r_0 = \frac{1}{2}\left[r_0(\text{bulk gas}) + (\text{lattice spacing between graphite planes})\right] = \frac{1}{2}\left[r_0^g + 3.40\text{Å}\right].$$

By numerically minimizing Eq. 1, the adsorbate–adsorbent interaction energy within a given pore is taken as the negative of this minimum potential (Jagiello and Schwarz, 1992, 1993; Hu and Do, 1994):

$$E(k, r_p) = u_p^*(k, r_p), \quad (2)$$

where u_p^* is the depth of the potential minimum, and it ranges from the value for the interaction potential minimum depth with a single wall ($r_p \to \infty$), u_s^*, to the value of $2u_s^*$ for $r_p = r_0$.

For multicomponent systems, the local adsorption isotherm for a given micropore is represented by the IAST, with the pure component isotherm following the Langmuir equation:

$$C_\mu^0(k, r_p) = C_{\mu s}(k)\frac{b_0(k)e^{E(k,r_p)/R_gT}C_p(k)}{1 + b_0(k)e^{E(k,r_p)/R_gT}C_p(k)}, \quad (3)$$

where $C_{\mu s}$ is the adsorption saturation capacity; C_p is the gas-phase concentration; R_g is the gas constant; T is temperature, b_0 is the adsorption affinity at zero energy level; and $E(k, r_p)$ is the adsorbate-pore interaction energy for adsorbate k.

The observed adsorption isotherm on the adsorbent can be expressed as the integral of the local isotherm, $C_\mu(k, r_p)$, over the pore-size range accessible to the adsorbate:

$$C_\mu(k) = \int_{r_{\min}(k)}^{\infty} C_\mu(k, r_p)\,F(r_p)\,dr_p, \quad (4)$$

where $r_{\min}(k)$ is the minimum half-width of the pore accessible to adsorbate k; $F(r_p)$ is the micropore-size distribution, which is assumed to follow a gamma distribution:

$$F(r_p) = \frac{q^{\nu+1}r_p^\nu e^{-qr_p}}{\Gamma(\nu+1)}, \quad (5)$$

where q, ν are the two distribution parameters.

The effect of size exclusion is reflected in the lower integration limit, and in the iterative calculation of local equilibria with IAST, a species j with a molecular size larger than the lower integration limit, $r_{\min}(k)$ of Eq. 4, cannot be adsorbed for those micropores between $r_{\min}(k)$ and $r_{\min}(j)$.

The local surface diffusion flux

The driving force for the diffusion of adsorbed species is assumed to be the chemical potential gradient, hence the local surface diffusion flux of species k, $J_\mu(k, r_p)$, can be written as (Hu and Do, 1992):

$$J_\mu(k, r_p) = -D_\mu(k, r_p)\frac{C_\mu(k, r_p)}{C_p(k)}\frac{\partial C_p(k)}{\partial r}, \qquad (6)$$

where r is the coordinate in the particle, and D_μ is the zero coverage surface diffusivity and related to the micropore half-width by

$$D_\mu(k, r_p) = D_{\mu 0}(k)\exp\left(-\frac{a(k)E(k, r_p)}{R_g T}\right), \qquad (7)$$

where a is the ratio of surface activation energy to the adsorption energy, $D_{\mu 0}$ is the zero coverage surface diffusivity at zero energy level.

Mass-balance equations

Since the particle is large, the mass transfer can be assumed to be under pore and surface diffusion control, so the mass-balance equation for species k in the particle is

$$\epsilon_M\frac{\partial C_p(k)}{\partial t} + (1-\epsilon_M)\frac{\partial}{\partial t}\int_{r_{\min(k)}}^{\infty} C_\mu(k, r_p)F(r_p)\,dr_p = -\epsilon_M\frac{1}{r^s}$$
$$\times\frac{\partial}{\partial r}\left(r^s J_p(k)\right) - (1-\epsilon_M)\frac{1}{r^s}\frac{\partial}{\partial r}\left(r^s\int_{r_{\min(k)}}^{\infty} J_\mu(k, r_p)F(r_p)\,dr_p\right), \qquad (8)$$

where ϵ_M is the macropore porosity; s is the particle geometric factor having a value of 0, 1, or 2 for slab, cylinder, or sphere, respectively; and J_p is the macropore diffusion flux and is usually defined as (Ruthven, 1984):

$$J_p(k) = -D_p(k)\frac{\partial C_p(k)}{\partial r}, \qquad (9)$$

where D_p is the pore diffusivity, calculated from the combined molecular and Knudsen diffusivities and the tortuosity of the adsorbent.

In Eq. 8, the diffusion rate of adsorbed species in the particle and the local adsorbed concentration are related to the gas concentrations $\{Cp(j);\ j = 1, 2, \ldots, NC\}$ by the multicomponent adsorption equilibrium relation (iteratively calculated from the IAST), the effects of size exclusion are accounted for in the lower integration limit, and in the iterative calculation of IAST.

One of the boundary conditions of Eq. 8 is the zero flux at the particle center:

$$r = 0; \quad \frac{\partial C_p(k)}{\partial r} = 0; \quad \frac{\partial C_\mu(k)}{\partial r} = 0. \qquad (10)$$

Another boundary condition is at the particle exterior surface:

$$r = R; \quad \epsilon_M J_p(k) + (1-\epsilon_M)\int_0^{\infty} J_\mu(k, r_p)F(r_p)\,dr_p$$
$$= k_m(k)\left[C_p(k) - C_b(k)\right], \qquad (11)$$

where k_m is the film mass transfer coefficient, R is the radius (half-width) of the particle and C_b is the adsorbate concentration in the bulk phase.

The initial conditions of the model equations are

$$t = 0; \quad C_p(k) = C_{pi}(k); \quad C_\mu(k) = C_{\mu i}(k). \qquad (12)$$

Here the initial concentrations of all species in both pore and adsorbed phases are assumed uniform.

Method of solution

To facilitate the analysis, the preceding model equations are cast into nondimensional form along the same line as Hu et al. (1999). The resulting nondimensional equations are solved by a combination of the orthogonal collocation method (Villadsen and Michelsen, 1978) and a DAE integration routine (Petzold, 1982). In the iterative calculation of IAST, an integration technique using a Gaussian quadrature to numerically calculate the reduced spreading pressure from the single-gas isotherm equation has been applied to save computing time (Hu and Do, 1992).

Experimental

The isotherm data were collected using a volumetric measurement rig, and the kinetics responses were obtained using a differential adsorber bed (DAB). Two commercial activated carbons, Norit and Ajax, were used as the adsorbents in this study, and ethane and propane were used as the adsorbates. The physical and structural properties of the adsorbents and the measurement procedures of adsorption isotherm and kinetics were given in the earlier work of Hu and coworkers (Hu et al., 1994; Hu and Do, 1993; Qiao and Hu, 1999). The system pressure used in all kinetics runs is 1 atm. The dilution gas used is helium for Norit carbon and nitrogen for Ajax carbon.

Results and Discussion

Micropore-size distribution of the activated carbon

Figure 1 shows graphically the MPSD of Norit and Ajax activated carbons. The micropore-size distribution data measured by the Horvath-Kawazoe method are presented as symbols. A gamma function is assumed in this article to describe the pore-size distribution, although other function forms can also be used. The fitting results using a nonlinear regression

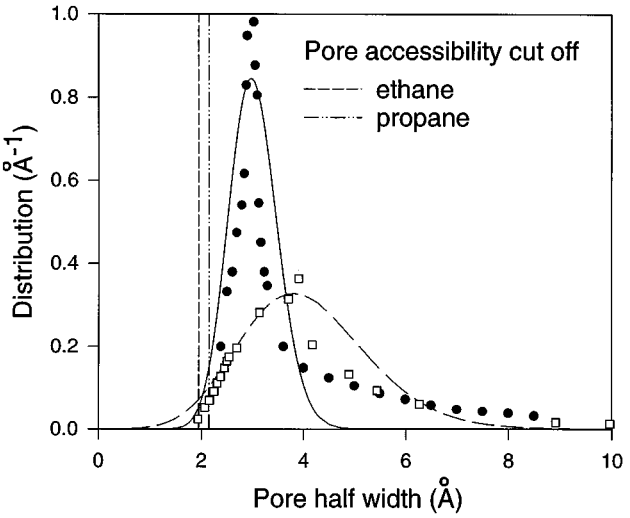

Figure 1. Micropore-size distribution of Ajax and Norit activated carbons.

(●) MPSD of Norit carbon by H-K method; (□) MPSD of Ajax carbon by H-K method; (——) gamma distribution fitting for Norit carbon; (– – –) gamma distribution fitting for Ajax carbon.

based on the least-square technique are plotted as a solid line for Norit carbon and a dashed line for Ajax carbon, respectively. The optimal micropore-size distribution parameters are $q = 21.01$ Å^{-1}, $\upsilon = 98.14$ for Norit carbon (Qiao et al., 2000a) and $q = 3.732$ Å^{-1}, $\upsilon = 20.53$ for Ajax carbon (Hu et al., 1999). The molecule diameter of adsorbate dictates the accessibility of that species in the micropore network of the

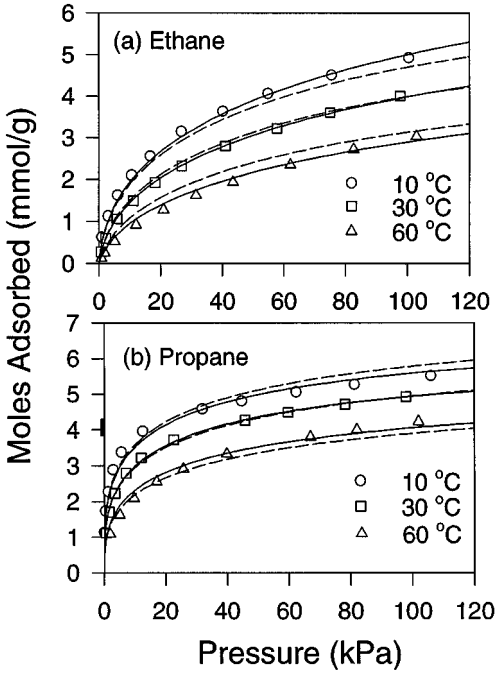

Figure 2. Adsorption isotherm data and model fitting of ethane and propane on Ajax activated carbon.

(____) Different $C_{\mu s}$; (– – –) same $C_{\mu s}$.

Table 1. Isotherm Parameters, Pore, and Surface Diffusivities for Ethane and Propane on Ajax Carbon

T	$C_{\mu s}$ (kmol/m^3)		$b_o \times 10^2$ (kPa^{-1})		u_s^* (kJ/mol)		$D_{\mu 0} \times 10^7$ (m^2/s)		$D_p \times 10^6$ (m^2/s)	
(°C)	C_2	C_3	C_2	C_3	C_2	C_3	C_2	C_3	C_2	C_3
10	9.230	6.852							1.51	1.20
30	7.691	6.197	0.127	0.197	8.171	12.84	0.184	0.165	1.68	1.30
60	5.954	5.267							1.96	1.56

Note: Different $C_{\mu s}$ for different species.

adsorbent. In this study we use the values reported by Breck (1974). The molecule diameters of ethane and propane are 3.9 and 4.3 Å. The minimal accessible pore half-widths, $r_{\min}$, of ethane and propane are also shown in Figure 1. Here $r_{\min}$ is defined as the half-width of pores in which the adsorption potential is zero ($r_{\min} = 0.8583 r_0$ for the 10-4 potential). It is seen that only a small number of pores of two activated carbons are excluded for ethane and propane molecules, respectively.

Adsorption isotherm

The isotherm parameters of adsorbates were obtained by fitting the model to the corresponding experimental equilibrium data of a single component at various temperatures simultaneously. During optimization, $C_{\mu s}$ is set both temperature and species dependent while the other two parameters, b_0 and u_s^*, are temperature independent but species dependent. Figure 2 shows the model fittings (solid lines) and the pure-component equilibrium data (symbols) of ethane and propane on Ajax activated carbon. It is seen that the model fits well the equilibrium data of both ethane and propane over the experimental concentration and temperature range. The derived isotherm parameters for the two species are tabulated in Table 1.

In the MPSD-EL model, since an extended Langmuir isotherm is used to describe the local multicomponent adsorption equilibrium, the maximum adsorption capacity is usually forced to be the same for all components to satisfy the thermodynamic consistence (Hu and Do, 1996; Hu, 1999). To study how this restriction affects the single-component data fitting and multicomponent kinetics prediction, another methodology is carried out to reoptimize the pure-component equilibrium parameters for ethane and propane with the preceding constraint, two species having the same maximum adsorption capacity enforced. The new parameters, listed in Table 2, are obtained by fitting the experimental data of two

Table 2. Isotherm Parameters, Pore, and Surface Diffusivities for Ethane and Propane on Ajax Carbon

T	$C_{\mu s}$ (kmol/m^3)		$b_o \times 10^2$ (kPa^{-1})		u_s^* (kJ/mol)		$D_{\mu 0} \times 10^7$ (m^2/s)		$D_p \times 10^6$ (m^2/s)	
(°C)	C_2	C_3	C_2	C_3	C_2	C_3	C_2	C_3	C_2	C_3
10	7.454								1.51	1.20
30	6.553		0.231	0.130	7.619	13.34	0.148	0.188	1.68	1.30
60	5.389								1.96	1.56

Note: Same $C_{\mu s}$ for different species.

Table 3. Isotherm Parameters, Pore, and Surface Diffusivities for Ethane and Propane on Norit Carbon

T (°C)	$C_{\mu s}$ (kmol/m^3)		$b_o \times 10^2$ (kPa^{-1})		u_s^* (kJ/mol)		$D_{\mu 0} \times 10^6$ (m^2/s)		$D_p \times 10^6$ (m^2/s)	
	C_2	C_3	C_2	C_3	C_2	C_3	C_2	C_3	C_2	C_3
30	10.21	5.074							2.12	1.75
60	9.904	4.520	0.011	1.528	17.99	12.81	4.357	0.336	2.26	1.86
90	9.532	3.979							2.36	1.97

Note: Different $C_{\mu s}$ for different species.

species at three different temperatures (a total of six isotherms) simultaneously. The model fittings with this constraint for ethane and propane are shown as dashed lines in Figure 2. It can be seen that the fitting is similar but slightly worse than the model without this restriction (solid lines). Both model fittings are within the experimental error of the data.

The pure-component isotherm parameters for ethane and propane on Norit activated carbon are also derived using the two optimization schemes just mentioned, respectively, which are shown in Tables 3 and 4. The isotherm parameters in Table 4 are obtained by fitting the experimental data of two adsorbates, ethane and propane, at three temperatures, 303, 333 and 363 K, simultaneously. Figure 3 shows the model fittings (lines) and the pure-component adsorption equilibrium data (symbols) of ethane and propane on Norit carbon. Again the MPSD model with variable $C_{\mu s}$ fits the pure-component isotherm data marginally better than the model using the same $C_{\mu s}$.

Single-component adsorption kinetics

The experimental kinetics data of ethane measured at three bulk-phase concentrations (5%, 10% and 20%) on Ajax activated carbon of a 4.4-mm full-length slab at 30°C are first utilized to optimize the model parameter, surface diffusivity at zero energy level, which is independent of concentration and temperature. The pore diffusivity is computed from the combined molecular and Knudsen diffusivities and a tortuosity of eight. The ratio of the activation energy for surface diffusion to the local interaction energy, a, is taken as 0.5. The extracted dynamic parameters of ethane adsorption for two cases, variable $C_{\mu s}$ and the same $C_{\mu s}$, are tabulated in Tables 1 and 2, respectively. The model fitting (solid lines for variable $C_{\mu s}$ and dashed lines for the same $C_{\mu s}$) and the experimental data (symbols) are shown in Figure 4a as the fractional uptake vs. time. The fractional uptake is defined as the uptake

Table 4. Isotherm Parameters, Pore, and Surface Diffusivities for Ethane and Propane on Norit Carbon

T (°C)	$C_{\mu s}$ (kmol/m^3)		$b_o \times 10^4$ (kPa^{-1})		u_s^* (kJ/mol)		$D_{\mu 0} \times 10^6$ (m^2/s)		$D_p \times 10^6$ (m^2/s)	
	C_2	C_3	C_2	C_3	C_2	C_3	C_2	C_3	C_2	C_3
30	5.196								2.12	1.75
60	4.479		1.679	1.964	11.39	12.30	0.383	0.294	2.26	1.86
90	3.813								2.38	1.97

Note: Same $C_{\mu s}$ for different species.

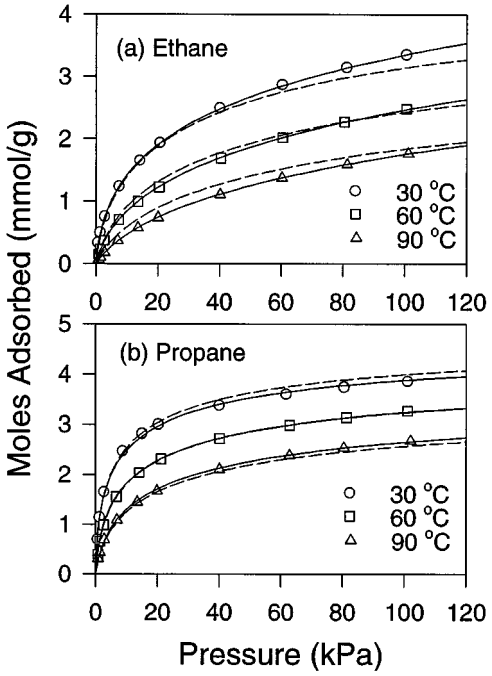

Figure 3. Adsorption isotherm data and model fitting of ethane and propane on Norit activated carbon.

(——) Different $C_{\mu s}$; (– – –) same $C_{\mu s}$.

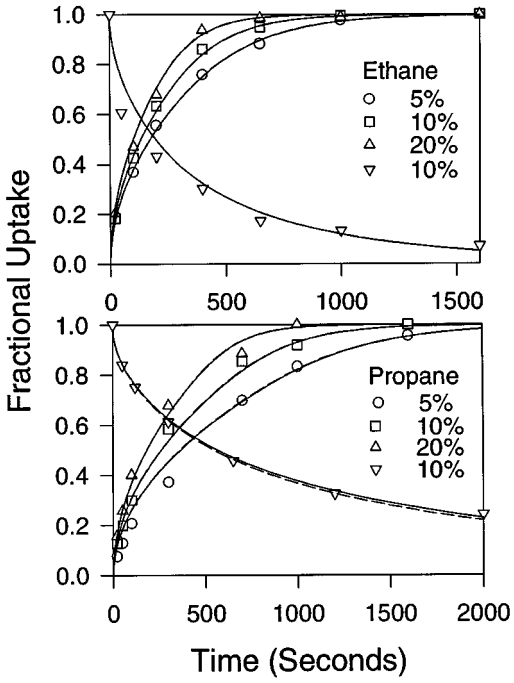

Figure 4. Single-component adsorption and desorption kinetics of ethane and propane on Ajax activated carbon of 4.4-mm full-length slabs at 30°C, 1 atm.

(——) Different $C_{\mu s}$; (– – –) same $C_{\mu s}$.

$$\left\{\frac{R^{s+1}}{S+1}\int_0^R\left[\epsilon_M C_p+(1-\epsilon_M)C_\mu\right]dr\right\}$$

at any time divided by its value at final equilibrium (time $=\infty$). It can be seen that the model fittings for the two cases are superimposed to each other and are in good agreement with the experimental uptake data. The concentration dependence of adsorption kinetics can be adequately described by the model.

After the zero coverage diffusivity at the zero energy level is obtained, the model is used to predict the desorption kinetics of 10% ethane on the same adsorbent at 30°C, which is also plotted in Figure 4a. It shows that prediction results of the two cases are again superimposed on each other and agree well with experimental data. It can be concluded that the effect of the two fitting schemes of pure-gas isotherm on the fitting of single-component adsorption kinetics is not significant.

Next, the model was employed to fit the adsorption kinetics of propane at three concentrations, 5, 10, and 20%, in a 4.4 mm full-length slab of Ajax activated carbon at 30°C and 1 atm simultaneously to extract the dynamic parameters of propane. The extracted dynamic parameters are also listed in Tables 1 and 2. These fitting results and the prediction for desorption of 10% propane on the same adsorbent are plotted in Figure 4b. It is seen that the models fit experimental data well and give an excellent prediction for propane desorption. Again the two cases, variable $C_{\mu s}$ and the same $C_{\mu s}$, offer similar fitting and prediction results.

The same procedures as just described are used to fit and simulate the experimental kinetics data of ethane and propane on Norit activated carbon of a 4.41-mm half-length slab at 30°C, 1 atm. The ratio of the activation energy for surface diffusion to the local interaction energy, *a*, is still taken as 0.5. The pore diffusivity of each species is computed from the combined molecular and Knudsen diffusivities and a tortuosity of three. The optimized values of $D_{\mu 0}$ for ethane and propane are listed in Tables 3 and 4, respectively, for different maximum adsorption capacity cases. Figure 5 presents the fitting and prediction results of ethane and propane sorption on Norit activated carbon. It is seen that the model fits the experimental adsorption data very well and can reasonably predict the desorption kinetics of ethane, although the simulated uptake is a little bit faster than the experimental data. Some deviations are found for the desorption simulation of propane, especially when the fractional uptake of propane becomes less than 0.5.

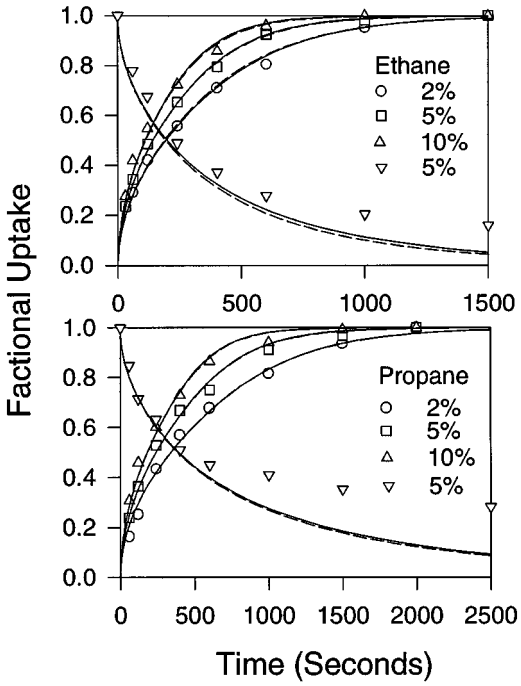

Figure 5. Single-component adsorption and desorption kinetics of ethane and propane on Norit activated carbon of 4.41-mm half-length slabs at 30°C, 1 atm.

(——) Different $C_{\mu s}$; (– – –) same $C_{\mu s}$.

Binary adsorption kinetics

Three models are employed in this subsection to predict the binary adsorption kinetics data measured on the two activated carbons by using the related equilibrium and kinetics information of the pure-component system only. They are (1) the MPSD-IAST model; (2) the MPSD-EL model assuming different $C_{\mu s}$ for various species; and (3) the MPSD-EL model assuming the same $C_{\mu s}$ for all species. Models 1 and 2 have the same single-component isotherm and kinetics parameters, which are listed in Table 1 for Ajax carbon and Table 3 for Norit carbon, respectively. For model 3 the pure-component equilibrium and kinetics parameters are listed in Tables 2 and 4 for Ajax and Norit carbons, respectively.

The three models are first employed to simulate the binary adsorption kinetics data of ethane and propane on Ajax activated carbon. The adsorption kinetics of the binary mixtures of ethane and propane is measured on Ajax activated carbon of the 4.4-mm full-length slab at three bulk-phase compositions: (1) ethane (5%)–propane (5%); (2) ethane (10%)–propane (5%); and (3) ethane (20%)–propane (5%). The bulk-phase pressure is 1 atm and the temperature is 10°C. Figure 6 shows these adsorption experimental data (symbols) and the related model predictions (lines). The solid lines show the prediction results of the MPSD-IAST model, the dashed lines show the MPSD-EL model with variable $C_{\mu s}$ and the dashed-dotted lines show the MPSD-EL model with the same $C_{\mu s}$. Since the system consists of a fast-moving/less strongly adsorbed species (ethane) and a slow-moving/more strongly adsorbed species (propane), the typical overshoot maximum in ethane uptake curve is observed. The MPSD-IAST model and the MPSD-EL model with the same $C_{\mu s}$ give similar predictions, but the MPSD-EL model with variable $C_{\mu s}$ overpredicts the overshoot degree of ethane uptake. The reason is possibly that for variable $C_{\mu s}$, in this case, the saturation capacity of ethane (9.230 mmol/mL) is significantly different from that of propane (6.852 mmol/mL), the extended Langmuir equation violates the thermodynamics, resulting in some error. Because propane is the slow-diffusing/more strongly

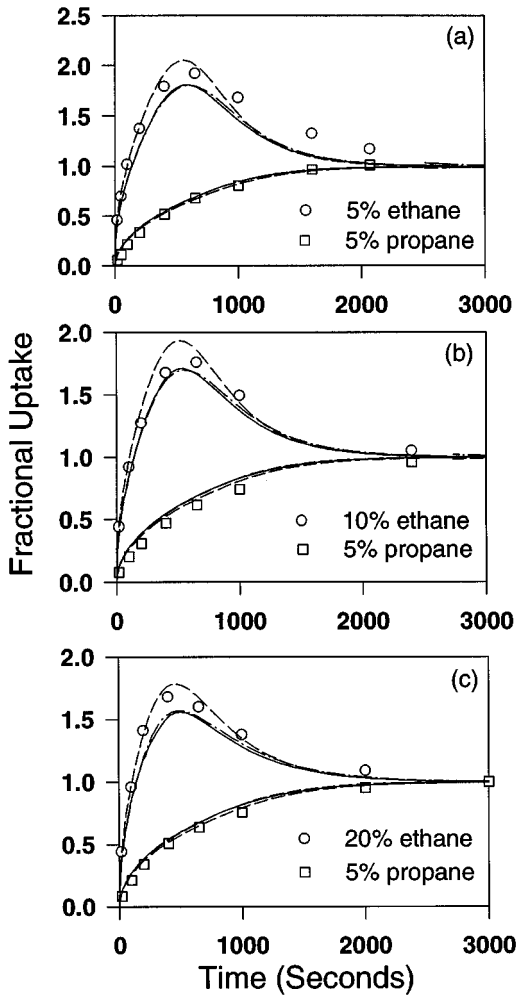

Figure 6. Binary adsorption kinetics of ethane and propane on Ajax activated carbon of 4.4-mm full-length slabs at 10°C, 1 atm.

(——) MPSD-IAST; (– – –) MPSD-EL (different $C_{\mu s}$); (–·–·–) MPSD-EL (same $C_{\mu s}$).

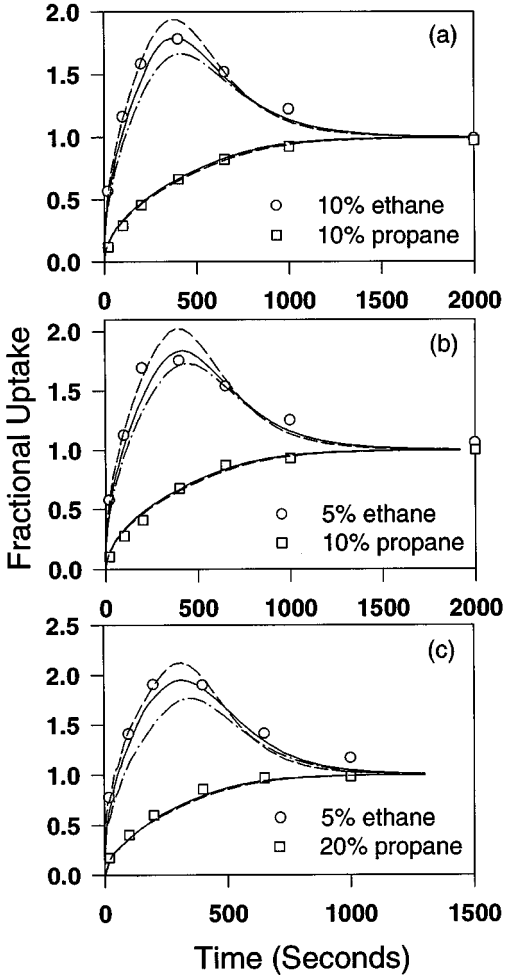

Figure 7. Binary adsorption kinetics of ethane and propane on Ajax activated carbon of 4.4-mm full-length slabs at 30°C, 1 atm.

(——) MPSD-IAST; (– – –) MPSD-EL (different $C_{\mu s}$); (–·–·–) MPSD-EL (same $C_{\mu s}$).

adsorbed species, it behaves like single-component so that the model predictions on propane uptake are superimposed on each other and are in good agreement with experimental data.

The proposed model is further tested with the binary adsorption kinetics of ethane and propane in Ajax activated carbon of the 4.4-mm full-length slab at another temperature, 30°C, under different concentration combinations, which are shown in Figures 7 and 8. The MPSD-IAST model best predicts the overshoot degree of ethane, while the MPSD-EL model with different $C_{\mu s}$ overpredicts the ethane uptake, and with the same $C_{\mu s}$ underpredicts the ethane uptake.

To further examine the model potential, the models are used to predict the binary adsorption kinetics of hydrocarbons on another activated carbon (Norit carbon). Figure 9 shows the simultaneous adsorption kinetics of 5% propane together with different concentrations of ethane (2, 5, and 10%) on the 4.41-mm half-length slab particles of Norit carbon at 30°C, 1 atm. The predictions of this study (MPSD-IAST model, solid lines) are in reasonable agreement with the experimental data (symbols). Again, the MPSD-EL model with different $C_{\mu s}$ (dashed lines) overpredicts the overshoot of ethane uptake. The reason is that the saturation adsorption capacity of ethane (10.205 mmol/mL) is about twice of that of propane (5.074 mmol/mL), so it can cause a significant deviation by using the extended Langmuir isotherm equation. The MPSD-EL model with the same $C_{\mu s}$ (dashed-dotted lines) well predicts the adsorption kinetics. This implies that with special treatment in the pure-component equilibrium data analysis, that is, forcing the saturation capacities of different species to be the same, the thermodynamic consistency is satisfied and the MPSD-EL model's prediction for the light species is improved. But this improvement also depends on the fact that the model's capability in fitting the pure-component isotherm data is not seriously discounted. As seen in Figure 3, the isotherm fitting is still good enough at 30°C after the saturation capacities of ethane and propane are forced to be the same.

Figure 10 shows the simultaneous adsorption kinetics of 5% ethane together with different concentrations of propane

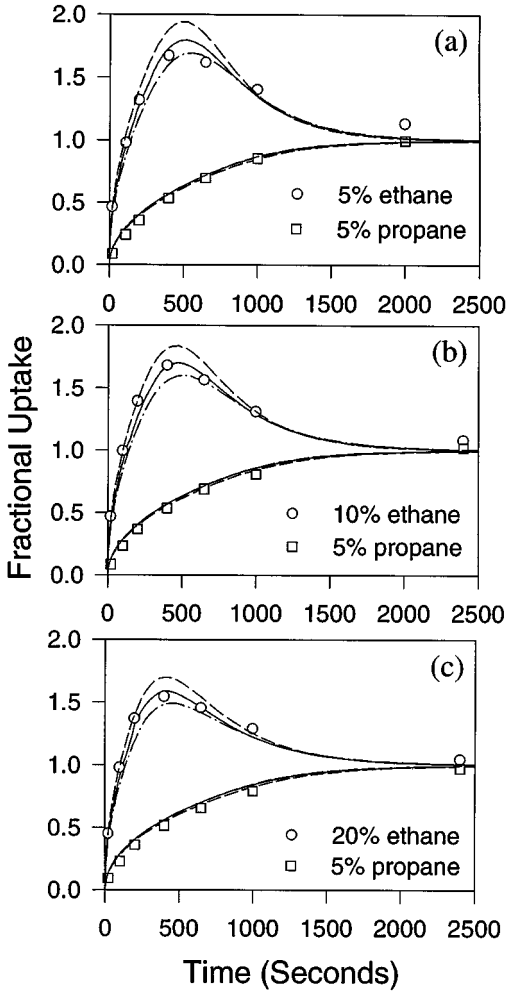

Figure 8. Binary adsorption kinetics of ethane and propane on Ajax activated carbon of 4.4-mm full-length slabs at 30°C, 1 atm.

(——) MPSD-IAST; (– – –) MPSD-EL (different $C_{\mu s}$); (–·–·–) MPSD-EL (same $C_{\mu s}$).

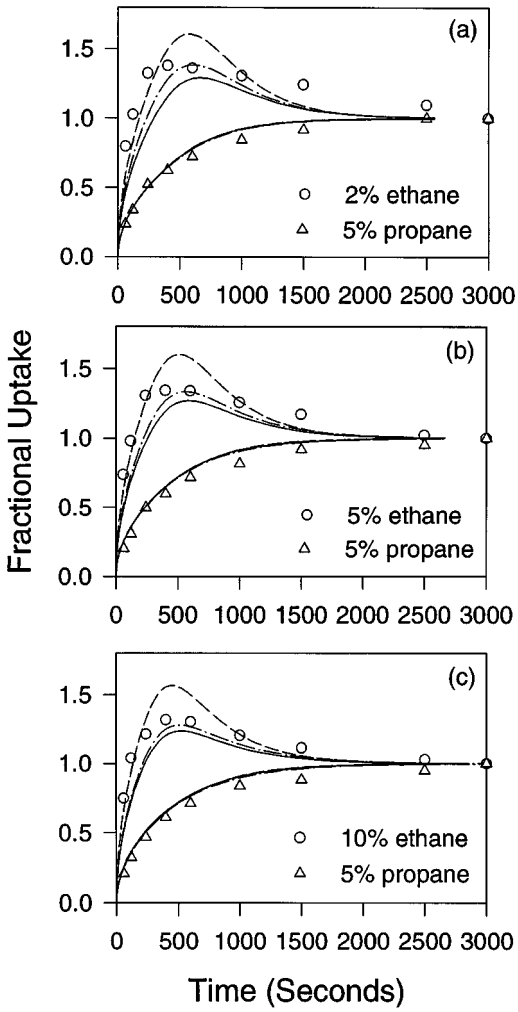

Figure 9. Binary adsorption kinetics of ethane and propane on Norit activated carbon of 4.41-mm half-length slab at 30°C, 1 atm.

(——) MPSD-IAST; (– – –) MPSD-EL (different $C_{\mu s}$); (–·–·–) MPSD-EL (same $C_{\mu s}$).

(2% and 10%) on the same adsorbent particle at 30°C, 1 atm. Similar phenomena as in Figure 9 are observed.

Binary desorption kinetics

Finally, to carry out a more rigorous test on the MPSD-IAST model, the simultaneous desorption kinetics of the binary ethane–propane system on Ajax and Norit activated carbons is investigated. Binary desorption dynamics of 10% ethane and 10% propane on the 4.4-mm full-length slabs of Ajax activated carbon at 30°C and 1 atm was first measured. The experimental data (symbols) are shown in Figure 11 together with the corresponding predictions of this work (MPSD-IAST, solid lines) and the MPSD-EL models (dashed line for different $C_{\mu s}$, dashed-dotted lines for the same $C_{\mu s}$). It is seen that the prediction results of three models are close to each other and are in good agreement with experimental data.

The desorption kinetics of two binary mixtures of ethane (5%)–propane (5%) and ethane (5%)–propane (10%) on Norit carbon of the 4.41-mm half-length slabs at 30°C and 1 atm were also measured and compared with the model simulations. Figure 12 shows the model predictions (lines) and the experimental data (symbols) of these two gas mixtures. The model prediction for ethane using the MPSD-IAST model gives a better result than the two MPSD-EL models. Because propane is the slow-diffusing/more strongly adsorbed species, the three models give similar results for the propane uptake rate prediction.

To examine the temperature dependence of the model, the desorption kinetics of the binary mixture of ethane (5%)–propane (5%) on Norit carbon at a higher temperature of 60°C, 1 atm are then measured and compared with the simulation results, which are shown in Figure 13. Phenomena similar to those in Figure 12 are observed.

Conclusions

A new multicomponent adsorption kinetics model is proposed using a micropore-size distribution to represent the

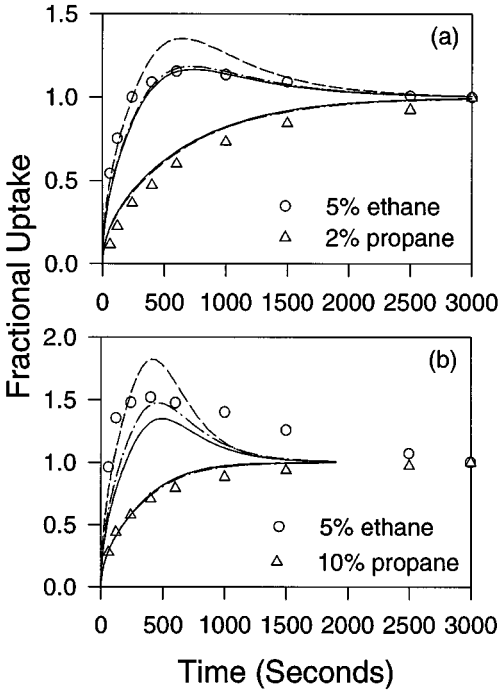

Figure 10. Binary adsorption kinetics of ethane and propane on Norit activated carbon of 4.41-mm half-length slabs at 30°C, 1 atm.

(——) MPSD-IAST; (– – –) MPSD-EL (different $C_{\mu s}$); (–·–·–) MPSD-EL (same $C_{\mu s}$).

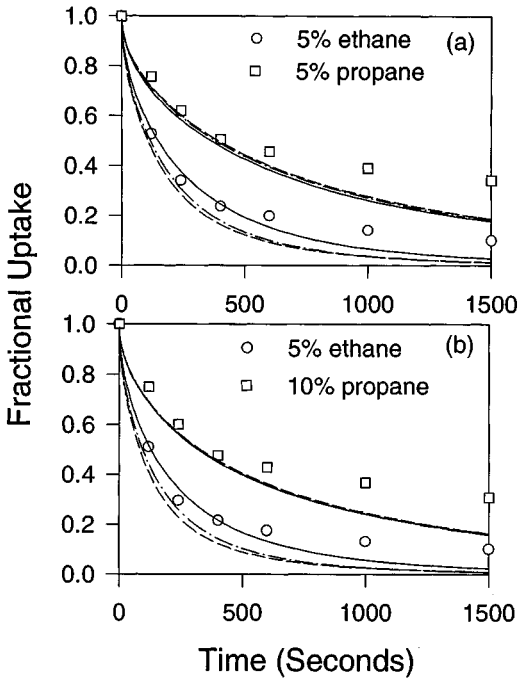

Figure 12. Binary desorption kinetics of ethane and propane on Norit activated carbon of 4.41-mm half-length slabs at 30°C, 1 atm.

(——) MPSD-IAST; (– – –) MPSD-EL (different $C_{\mu s}$); (–·–·–) MPSD-EL (same $C_{\mu s}$).

energetic heterogeneity of the adsorbent and the ideal adsorbed solution theory to describe the local multicomponent adsorption equilibrium. The size exclusion effect is taken into account in the competition of different species for a given pore. The MPSD-IAST model can fit the single-component adsorption isotherm well and is thermodynamically consistent in the prediction of multicomponent adsorption equilibrium and kinetics. It overcomes the drawbacks in the MPSD-EL model that either the single-component isotherm data fitting is not good enough when the saturation adsorption capacity is forced to be the same for all species or the different saturation adsorption capacities for different species violate the thermodynamics. The MPSD-IAST model is validated with experimental kinetics data on Ajax and Norit activated carbons. It is found that, using the pure-component equilibrium and kinetics information, the MPSD-IAST kinetics model is able to predict binary adsorption kinetics reliably under the experimental conditions.

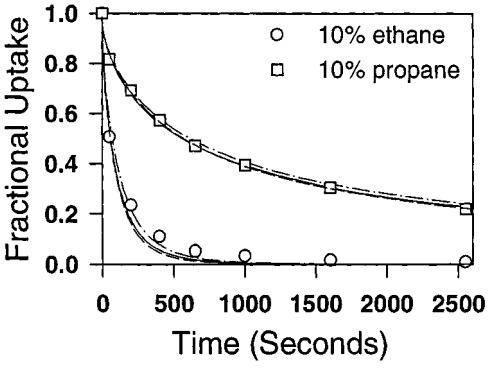

Figure 11. Binary desorption kinetics of 10% ethane and 10% propane on Ajax activated carbon of 4.4-mm full-length slabs at 30°C, 1 atm.

(——) MPSD-IAST; (– – –) MPSD-EL (different $C_{\mu s}$); (–·–·–) MPSD-EL (same $C_{\mu s}$).

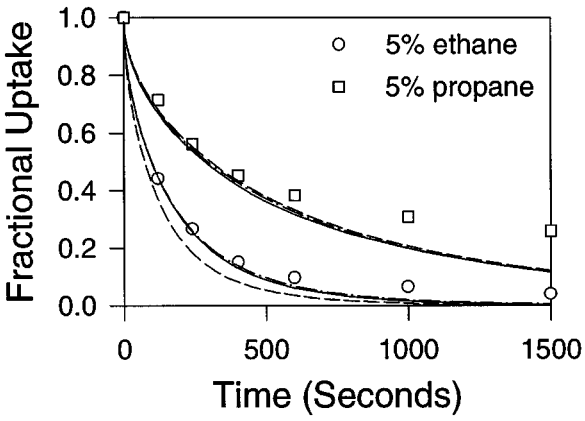

Figure 13. Binary desorption kinetics of 5% ethane and 5% propane on Norit activated carbon of 4.41-mm half-length slabs at 60°C, 1 atm.

(——) MPSD-IAST; (– – –) MPSD-EL (different $C_{\mu s}$); (–·–·–) MPSD-EL (same $C_{\mu s}$).

Acknowledgments

The work described in this article was substantially supported by a grant from the Research Grants Council of the Hong Kong Special Administrative Region, China (Project No. HKUST6114/97P).

Notation

C_2 = ethane
C_3 = propane
C_μ = adsorbed concentration in the particle (kmol/m^3)
t = time (s)
Γ = gamma function

Literature Cited

Breck, D. W., *Zeolite Molecular Sieves: Structure, Chemistry and Use*, Wiley, New York (1974).

Do, D. D., and K. Wang, ''Dual Diffusion and Finite Mass Exchange Model for Adsorption Kinetics in Activated Carbon,'' *AIChE J.*, **44**, 68 (1998a).

Do, D. D., and K. Wang, ''A New Model for the Description of Adsorption Kinetics in Heterogeneous Activated Carbon,'' *Carbon*, **36**, 1539 (1998b).

Dunne, J., and A. L. Myers, ''Adsorption of Gas Mixtures in Micropores: Effect of Difference in Size of Adsorbate Molecules,'' *Chem. Eng. Sci.*, **49**, 2941 (1994).

Everett, D. H., and J. C. Powl, ''Adsorption in Slit-Like and Cylindrical Micropores in the Henry's Law Region,'' *J. Chem. Soc. Faraday Trans. I.*, **72**, 619 (1976).

Hu, X., ''Multicomponent Adsorption Equilibrium of Gases in Zeolite: Effect of Pore Size Distribution,'' *Chem. Eng. Comm.*, **174**, 201 (1999).

Hu, X., and D. D. Do, ''Multicomponent Adsorption Kinetics of Hydrocarbons onto Activated Carbon: Effect of Adsorption Equilibrium Equations,'' *Chem. Eng. Sci.*, **47**, 1715 (1992).

Hu, X., and D. D. Do, ''Effect of Surface Energetic Heterogeneity on the Kinetics of Adsorption of Gases in Microporous Activated Carbon,'' *Langmuir*, **9**, 2530 (1993).

Hu, X., and D. D. Do, ''Effect of Surface Heterogeneity on the Adsorption Kinetics of Gases in Activated Carbon: Pore Size Distribution vs. Energy Distribution,'' *Langmuir*, **10**, 3296 (1994).

Hu, X., and D. D. Do, ''Comparing Various Multicomponent Adsorption Equilibrium Models,'' *AIChE J.*, **41**, 1585 (1995a).

Hu, X., and D. D. Do, ''Validity of Isothermality in Adsorption Kinetics of Gases in Bidispersed Solids,'' *AIChE J.*, **41**, 1581 (1995b).

Hu, X., and D. D. Do, ''Effect of Pore Size Distribution on the Prediction of Multicomponent Adsorption Equilibria,'' *Fundamentals of Adsorption*, M. D. LeVan, ed., Kluwer, Boston, p. 385 (1996).

Hu, X., B. King, and D. D. Do, ''Ternary Adsorption Kinetics of Gases in Activated Carbon,'' *Gas Sep. Purif.*, **8**, 175 (1994).

Hu, X., S. Qiao, and D. D. Do, ''Multicomponent Adsorption Kinetics of Gases in Activated Carbon: Effect of Pore Size Distribution,'' *Langmuir*, **15**, 6428 (1999).

Jagiello, J., and J. A. Schwarz, ''Energetic and Structural Heterogeneity of Activated Carbons Determined Using Dubinin Isotherms and an Adsorption Potential in Model Micropores,'' *J. Colloid Interface Sci.*, **154**, 225 (1992).

Jagiello, J., and J. A. Schwarz, ''Relationship Between Energetic and Structural Heterogeneity of Microporous Carbons Determined on the Basis of Adsorption Potentials in Model Micropores,'' *Langmuir*, **9**, 2513 (1993).

Kapoor, A., J. A. Ritter, and R. T. Yang, ''An Extended Langmuir Model for Adsorption of Gas Mixtures on Heterogeneous Surfaces,'' *Langmuir*, **6**, 660 (1990).

Malek, A., and S. Farooq, ''Comparison of Isotherm Models for Hydrocarbon Adsorption on Activated Carbon,'' *AIChE J.*, **42**, 3191 (1996).

Moon, H., and C. Tien, ''Adsorption of Gas Mixture on Adsorbents with Heterogeneous Surface,'' *Chem. Eng. Sci.*, **43**, 2967 (1988).

Myers, A. L., and J. M. Prausnitz, ''Thermodynamics of Mixed-gas Adsorption,'' *AIChE J.*, **11**, 121 (1965).

Petzold, L. R., ''A Description of DASSL: A Differential/Algebraic Equation System Solver,'' Sandia Tech. Rep. SAND 82-8637, Livermore, CA (1982).

Qiao, S., and X. Hu, ''Binary Adsorption Kinetics of Ethane and Propane in a Large Heterogeneous Microporous Partile,'' *Sep. Purif. Technol.*, **16**, 261 (1999).

Qiao, S., and X. Hu, ''Effect of Micropore Size Distribution Induced Heterogeneity on Binary Adsorption Kinetics of Hydrocarbons in Activated Carbon,'' *Chem. Eng. Sci.*, **55**, 1533 (2000).

Qiao, S., K. Wang, and X. Hu, ''Study of Binary Adsorption Equilibrium of Hydrocarbons in Activated Carbon Using Micropore Size Distribution,'' *Langmuir*, **16**, 5130 (2000a).

Qiao, S., K. Wang, and X. Hu, ''Using Local IAST with Micropore Size Distribution to Predict Multicomponent Adsorption Equilibrium of Gases in Activated Carbon,'' *Langmuir*, **16**, 1292 (2000b).

Ruthven, D. M., *Principles of Adsorption and Adsorption Processes*, Wiley, New York (1984).

Sircar, S., ''Influence of Adsorbate Size and Adsorbent Heterogeneity on IAST,'' *AIChE J.*, **41**, 1135 (1995).

Valenzuela, D. P., A. L. Myers, O. Talu, and I. Zwiebel, ''Adsorption of Gas Mixtures: Effect of Energetic Heterogeneity,'' *AIChE J.*, **34**, 397 (1988).

Villadsen, J., and M. L. Michelsen, *Solution of Partial Differential Equation Models by Polynomial Approximation*, Prentice Hall, Englewood Cliffs, NJ (1978).

Wang, K., and D. D. Do, ''Characterizing the Micropore-Size Distribution of Activated Carbon Using Equilibrium Data of Many Adsorbates at Various Temperatures,'' *Langmuir*, **13**, 6226 (1997).

Wang, K., S. Qiao, and X. Hu, ''Application of IAST in the Prediction of Multicomponent Adsorption Equilibrium of Gases in Heterogeneous Solids: Micropore Size Distribution vs Energy Distribution,'' *Ind. Eng. Chem. Res.*, **39**, 527 (2000).

Manuscript received Oct. 19, 1999, and revision received Mar. 29, 2000.